Cell Detection by a Microfluidic-Integrated Broadband Biosensor

Caroline Multari*, Yaqing Ning*, Xi Luo*, Cristiano Palego**, Agnese Denzi***, Caterina Merla****, Francesca Apollonio***, Micaela Liberti***, James C. M. Hwang* and Xuanhong Cheng*

* Lehigh University, 5 E. Packer Ave, Bethlehem, PA
** Bangor University, Gwynedd LL57 1UT UK
*** Sapienza University, Rome 00184 Italy
**** National Agency for New Technology, Energy and Sustainable Economic Development, Rome 00196 Italy

ABSTRACT

Detection of identity, quantity and viability of cells at the point-of-need is critically needed for diagnostic, surveillance and monitoring purposes. In this work, we present a broadband electrical sensor combined with a microfluidic device to detect mammalian cells and bacteria. It is found that the device can detect down to single mammalian cells in a suspension. The device is also capable of differentiating cells based on their viability and size. With a specific cell type, cell number can be obtained through signal analysis. Compared to conventional impedance sensors that operate in narrow and low frequency ranges, this device not only detects the properties of cell membranes in the MHz range, but also the intracellular environment in the GHz range, thus revealing richer information about the cell identity and function. Ongoing research intends to optimize the sensor performance to extract biochemical signature from cells.

Keywords: microfluidic, broadband, biosensor, cells

1 INTRODUCTION

Point-of-need identification of pathogenic cells and their activities is critically needed in clinical diagnosis, defense surveillance, and food/pharmaceutical safety monitoring. Although state-of-the-art technologies for pathogen detection are highly sensitive and specific, these tests are generally based on molecular analysis and cell culture, both of which require sophisticated instruments, specialized laboratories, and well-trained technicians that are inaccessible at the point of need. Furthermore, analysis of cell activities usually requires days to weeks of culture, preventing a timely response for threat reduction or diagnostic decision.

Propelled by the advances in the semiconductor industry, compact biosensors based on electrical mechanisms have attracted a lot of interest and found various applications in basic research, clinical diagnosis and homeland security applications [1-3]. Electrical detection of cells and tissues promises label-free, nondestructive detection at high throughputs. A number of miniaturized impedance sensors are created to detect physical properties of cells, such as cell size, shape and membrane integrity [4-7]. These sensors usually use a narrow range of electrical frequency optimized for cells of interest. The impedance signals from different types of cells, representing the ability of cells to resist current flow or hold charges, tend to vary by amplitudes only and have similar waveform, thus lack cell type specificity. Differentiating the signals associated with cell properties or identities often requires careful calibration and complicated signal analysis, while the results can be obscured by background or other non-specific signals. Another shortcoming with these sensors is that at the operating frequency in the kHz to MHz range, the polarization layer from electrolyte deposition on the sensors could screen or obscure the impedance signal from cells [8]. The polarization layer is especially severe given the high ion concentration associated with physiological solutions.

Here, we report a biosensor that uses broadband electrical measurements to analyze mammalian cells and bacteria. An input signal with a wide frequency range from MHz to GHz is delivered to cells confined in a microfluidic detection volume. Signals reflected from and transmitted through the cells are simultaneously measured, which are used to interpret interaction of cells with the input signal. Not only do the broadband measurements acquire membrane responses to electrical signals in the MHz ranger as in conventional impedance measurements, they also offer some unique advantages through signals the GHz range. The high frequency signal penetrates the electrolyte polarization layer more effectively, thus allows more signals delivered to and reflected from the sample for sensitive detection. Additionally, since biomolecules can absorb electromagnetic energy at the GHz to THz range through molecular vibration and rotation, it is possible to obtain absorption spectra associated with molecular markers for specific detection of cell types and viability. Furthermore, the low and high frequency components in broadband signals can potentially interact with different compartments of biological cells without ionization or heating [9-11]: megahertz electrical signals interact with the cell membrane effectively, while lipid bilayers are transparent to signals at gigahertz and higher frequencies, thus allowing these signals to penetrate to the cytoplasm and interact with the intracellular compartments [12, 13].

This makes it possible to interrogate cytosol and the organelles.

Despite of these advantages, broadband electrical measurements face some challenges, one of which being strong absorption of GHz energy by water. Here, we control the dissipation of the input signal through microfluidic chambers of comparable dimension to the target cells, thus creating a reproducible microenvironment with limited aqueous solution [14, 15]. To achieve high detection sensitivity, planar surface electrodes are created for signal transduction and their impedance is carefully designed. Using this setup, we demonstrate that reflected signals in the GHz range are predictive of size, viability and quantity of cells. The detection sensitivity of the sensor is down to single mammalian cells and it is also sensitive to detect bacteria trapped from a suspension.

2 EXPERIMENTAL

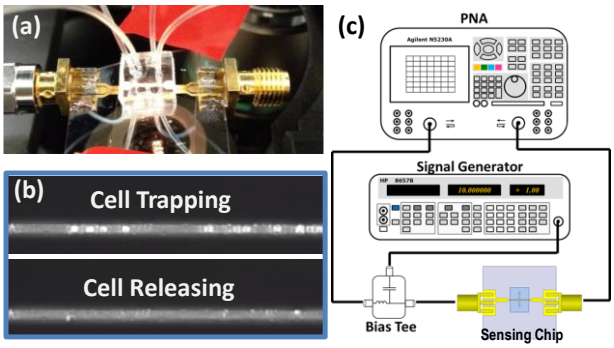

Figure 1. Experimental setup. (a) The biosensor comprises a gold micropatterned substrate bonded to a PDMS microchamber. The biosensor is inspected under an optical microscope to confirm the electrical measurements. (b) Bright field images showing temporary immobilization of cells between the electrodes for detection. (c) The sensing chip is connected to a signal generator for cell trapping and a network analyzer (PNA) for cell detection.

The biosensor comprises a sapphire substrate with micropatterned planar gold electrodes bonded to a microfluidic channel fabricated in polydimethylsiloxane (PDMS) (Fig. 1(a)). The two gold electrodes are approximately 100-µm wide, 2-µm thick and 10-µm apart. When a dielectric material such as a cell or buffer solution bridges the two electrodes, it influences the transduction of electrical signal along and between them, creating reflection and transmission spectra: the reflection spectrum is measured from the same end as the input signal and the transmission spectrum from the other end. Only the reflection signals are shown and analyzed in this paper. Both ends of the electrodes are connected to a vector network analyzer (PNA, Agilent N5230A), which emits broadband signal in the range of 10 MHz – 20 GHz and collects the output signals. The same electrodes are used to deliver a dielectrophoretic signal for temporary immobilization of cells (Fig. 1(b)). The trapping signal, on the order of 1 MHz and 1 V, is generated by a Hewlett Packard 8657B signal generator and is coupled to the broadband sensing signal. Dielectrophoresis signals of comparable frequency and strength were found to have little effect on cell morphology or function [16]. For mammalian cells, the number of trapped cells is controlled by the sample flow time and counted under an optical microscope (Fig. 1(c)). Since the concentrations of bacteria samples are generally much higher and the electrode separation is much greater than single bacterium, hundreds to thousands *E.coli* are trapped at the same time. The optical density between the electrodes is measured as an indicator of bacterium concentration in the detection zone.

Two human cell lines, Jurkat (immortalized T-lymphocyte line) and HEK 293 (embryonic kidney) cells are selected for comparison due to their differences in size, origin and culture state (~7 µm and suspension culture for Jurkat cells and ~15 µm and adhesion culture for HEK cells). Jurkat cells were cultured under 5% CO_2 at 37 ^{0}C in a media based on Sigma-Aldrich's RPMI 1640 with 10% fetal bovine serum, 100 units/ml penicillin, and 100 µg/ml streptomycin. HEK cells were cultured in DMEM high glucose with 10% fetal bovine serum, 100 units/ml penicillin, and 100 µg/ml streptomycin.

The *E. coli* strain used is PHL 628, which is genetically engineered to overexpress biofilm. The bacteria were cultured in LB with 50 µg/mL kanamycin at 30 °C. All cells measurements are performed with cells suspended in an isotonic sucrose solution.

The cells are delivered to the gold electrodes by the microfluidic channel, which is approximately 50-µm high, 250-µm wide and 5-mm long, and is bonded to the sapphire slide orthogonal to the gold electrodes. The flow rate on the order of 0.1 µl/min is controlled by a syringe pump.

For mammalian cell measurements, a fixed number of cells between 1 and 20 are immobilized first by the dielectrophoretic force followed with broadband sensing. After the measurement is performed, the trapping signal is turned off to release the cells and the measurement is repeated with the cell-free buffer. The difference is regarded as the net effect of the trapped cells. This referencing procedure is critical to minimize contribution from signal drifting caused by electrode polarization or environmental instability. Measurements are repeated with different numbers of trapped cells to determine the detection sensitivity and dynamic range. A similar procedure is applied to *E.coli* measurement except for much higher cell numbers

To minimize the effect of electrode polarization and ion shielding, all cells were washed with 8.5% sucrose plus 0.3% dextrose, then twice re-suspended in the sucrose solution before injection through the microfluidic channel. The working concentration of mammalian cells are ~3×10^6 cells/ml. The optical density of the re-suspended *E. coli* is ~0.27 at 600 nm. The sucrose solution is isotonic to ensure cell viability. To check viability of mammalian cells in the solution, Trypan Blue dye is used separately to confirm that

>50% of the cells survived after 10 h. Viability of the bacteria is confirmed through re-culture in suspension. To deliberately kill the cells, cells suspended in sucrose/dextrose solution were placed on a 115 ºC hot plate for 6 min. Death of mammalian cells was verified by Trypan Blue staining. Death of bacteria was verified by re-culturing for 24 hours.

3 RESULTS

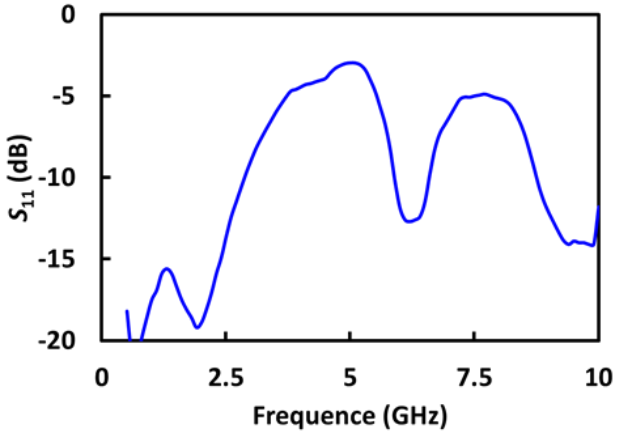

Figure 2. A typical raw S_{11} spectra from an isotonic sucrose solution.

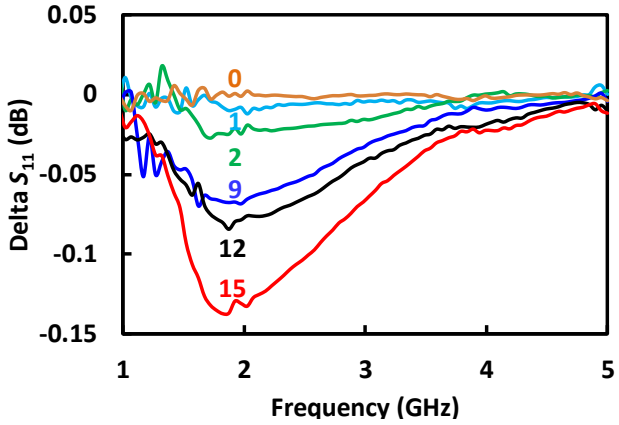

Figure 3. Reflected signals from different number of cells vs. frequency. Background signal without cells is subtracted to visualize signal contribution exclusively by cells.

Fig. 2 shows a typical reflection spectrum from a cell-free sucrose solution. The reflection signal is presented after normalization to the input signal and conversion to decibel, and is called S_{11} by convention. Deviation from 0 suggests transmission and dissipation of the electromagnetic energy by the material between the electrodes. Comparison of consecutive measurements with and without cells between the electrodes demonstrates that the sucrose solution alone generates repeatable reflection signals with a drift within 0.01 dB at most frequencies. On the other hand, the trapped cells induce different reflection signals from the buffer measurements in multiple frequency ranges. Such difference is observable even with single cell trapped between the electrodes, suggesting detection sensitivity in the single cell level.

To visualize reflection signals caused exclusively by cells, signals from cell-free measurements are subtracted from the cell measurements. Fig. 3 shows an example of subtracted reflection sginals in the frequency range of 1–5 GHz as a function of cell number. The cell-free signal is the baseline and the deviation is a result of signal dissipation/transmission by cells. As the cell number increases, the deviation aggrevates, indicating culmulative dispersion by multiple cells in parallel.

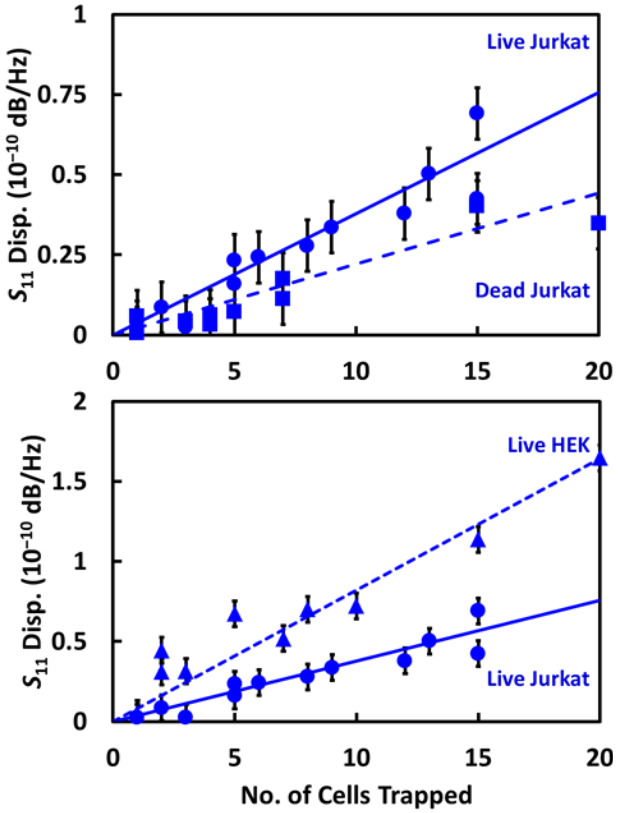

Figure 4. Measured changes of *S*-parameters dispersion in 2GHz - 3.5 GHz for different numbers of (a) live and dead Jurkat cells and (b) live Jurkat and HEK cells.

Since the subtracted signals in Fig. 3 appear linear in the frequency range of 2-3.5 GHz, linear regression is then used to average the signal in this frequency range and the slopes are compared relative to the number, viability and identity of cells. This slope represents the dispersion of the reflected signal per Hz of input. As seen in Fig. 4(a), the dispersion increases linearly with the number of trapped cells. Thus the dispersion has an additive effect from cells in series. As the cells die, the dispersion is dampened, but the linear relationship remains. Fitting the spectra in Fig. 2 to a circuit model suggests that the difference between live and dead cells is likely a result of the leakage of ions from the cytoplasm in the dead cells, which increases the cytoplasmic resistance by a few times. The model also predicts that the capacitance change associated with cell

death does not contribute to the observed signal difference, consistent with prior knowledge that lipid membranes are transparent to GHz frequency signals. This result of intracellular ion contribution is very different from conventional measurement using narrow band frequency in the kHz to MHz range, where the membrane capacitance shields the intracellular environment [17]. Broadband signals used here that span from MHz to GHz offer an opportunity to probe both membrane and intracellular environments in a non-invasive fashion.

When the dispersion is compared between two different types of cells (Fig. 4b), it is observed that the HEK cells generate approximately twice as much signal as Jurkat cells at the same cell number. This is consistent with HEK cells being approximately twice the size of Jurkat cells. Thus, the dispersion signal well correlates with physical properties of cells such as cell dimension and viability.

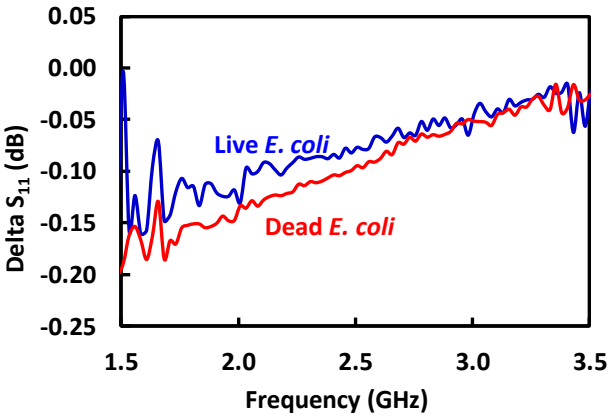

Figure 5. Reflected signals from live vs. dead *E. coli*

We further extend the biosensor to measure *E.coli* suspended in the sucrose solution. Visible bacteria enrichment is observed between the two electrodes when the trapping signal is turned on. When the reflection signal is compared between live and dead *E.coli*, a trend opposite to the mammalian cells is observed that dead bacteria reflect the input signal more strongly than the live ones (Fig. 5). Preliminary results also show that the signal intensity is dependent on the number of bacteria between the electrodes, with more cells generating stronger reflection. The different reflection signal with respect to cell viability between bacteria and mammalian cells may be a result of the cell wall structure in bacteria, while the mechanism is still under exploration.

4 CONCLUSIONS

We demonstrate here that a broadband electrical sensor is capable of differentiating physical properties of mammalian cells and bacteria, including cell number, viability and size. The detection reaches single cell sensitivity for mammalian cells. Compared to narrow band electrical sensing in the kHz-MHz range that is blocked by the cell membrane, the broadband signal up to 20 GHz interrogates both the cell membrane and intracellular environment. While current work focused on differentiating physical properties of cells, ongoing work is focused on improving the signal to noise ratio to detect biochemical signatures from molecular vibration. Such measurements are expected to reveal even richer information of target cells such as cell identity and function. Compact and capable of fast detection, the reported biosensor is expected to find tremendous application in point-of-need settings.

5 REFERENCES

[1] S. Y. Ho, G. S. Mittal, *Critical Reviews in Biotechnology* **16**, 349 (1996).

[2] J. J. Gooding, *Analytica Chimica Acta* **559**, 137 (2006).

[3] J. I. Hahm, *Journal of Biomedical Nanotechnology* **9**, 1 (2013).

[4] N. N. Watkins *et al.*, *Lab on a Chip* **11**, 1437 (2011).

[5] Y. S. Liu *et al.*, *Lab on a Chip* **7**, 603 (2007).

[6] D. Holmes *et al.*, *Lab on a Chip* **9**, 2881 (2009).

[7] H. Bayley, C. R. Martin, *Chemical Reviews* **100**, 2575 (Jul, 2000).

[8] H. P. Schwan, *Annals of the New York Academy of Sciences* **148**, 191 (1968).

[9] R. P. Joshi, J. Song, K. H. Schoenbach, V. Sridhara, *Ieee Transactions on Dielectrics and Electrical Insulation* **16**, 1243 (2009).

[10] P. T. Vernier, M. J. Ziegler, Y. H. Sun, M. A. Gundersen, D. P. Tieleman, *Physical Biology* **3**, 233 (2006).

[11] A. G. Pakhomov *et al.*, *Archives of Biochemistry and Biophysics* **465**, 109 (2007).

[12] C. Merla *et al.*, *IEEE Transactions on Biomedical Engineering* **49**, 2302 (2012).

[13] A. Denzi *et al.*, *J. Membrane Biology* **246**, 761(2013).

[14] A. C. Sabuncu, J. Zhuang, J. F. Kolb, A. Beskok, *Biomicrofluidics* **6**, 15 (2012).

[15] H. L. Gou *et al.*, *Journal of Chromatography A* **1218**, 5725 (2011).

[16] S. Archer, T. T. Li, A. T. Evans, S. T. Britland, H. Morgan, *Biochemical and Biophysical Research Communications* **257**, 687 (1999).

[17] Y. Ning, C. R. Multari, X. Luo, C. Merla, C. Palego, X. Cheng, and J. C. M. Hwang, *Proc. IEEE Int. Microwave Workshop Series RF Wireless Technologies Biomedical Healthcare Applications*, Singapore, Dec. 2013.

ACKNOWLEDGEMENTS

The project depicted is sponsored in part by the U.S. Department of Defense, Defense Threat Reduction Agency under Contract HDTRA1-12-1-0007. The content of the information does not necessarily reflect the position or the policy of the federal government, and no official endorsement should be inferred.